Gómez, M.J., Castejón, C., García-Prada, J.C. (2016). Crack detection in rotating shafts based on 3 × energy: Analytical and experimental analyses, *Mechanism and Machine Theory*, v. 96, Part 1, pp.: 94-106.

DOI: https://doi.org/10.1016/j.mechmachtheory.2015.09.009

Crack detection in rotating shafts based on 3x energy: analytical and experimental analyses

M.J. Gómez *, C. Castejón, J.C. García-Prada

MAQLAB Group, Mechanical Dept. University Carlos III of Madrid, Av. de la Universidad, 30, 28911, Leganés, Madrid, Spain

Abstract

Maintenance is essential to prevent catastrophic failures in rotating machinery. A crack can cause a failure with costly processes of reparation, especially in a rotating shaft.

In this study, the wavelet transform theory was applied to vibration signals to detect cracks in a rotating shaft. Data were obtained from an analytical Jeffcott rotor model with a breathing function to simulate cracks. Large changes in energy when a crack appears were discovered at 1x, 2x and 3x. Thereafter, vibration signals were obtained from a rotating machine at different steady-state rotational speeds using an accelerometer mounted on the bearing housing. Nine defect conditions were induced in the shaft (with depths from 4% to 50% of the shaft diameter). By matching the theoretical results with the experimental data, it was found that only the 3x component of the rotational speed is a clear indicator of the presence of a crack in this case. The energy level at this harmonic can be used for the inverse process of crack detection. Moreover, "probability of detection" curves were calculated. They showed very good results.

Key words:
Cracked shaft detection, Wavelet transform, Condition monitoring, Probability of Detection

1 Introduction

Cracked rotating shafts have received much attention over the last decades, and improved identification methods have allowed crack detection before the

* Corresponding author: mjggarci@ing.uc3m.es

occurrence of a failure under specific conditions. However, in some cases, detection is possible only when a system is close to a catastrophic failure, and there remains a need for the improvement of existing techniques based on the knowledge of the dynamical behavior of such a system.

Diagnosis techniques are usually classified into model-based and vibration methods [1]. It has been reported that while many papers have been published in this area, only few are based on real experimental results [2].

Model-based methods use equivalent loads to simulate effects of a defect; these methods are usually based on information extracted from directly measured signals, signal models and process models. This approach has been used in previous studies as [3–5].

On the other hand, vibration methods are based on the detection of variations in dynamical response when a crack appears. Sabnavis et al. [6] have reported that, at steady state, 1x and 2x vibrational frequencies can experiment important changes in energy in the presence of a crack. However, detection is difficult in practice because of noise and effects of other elements in a rotating machine, among other factors. Vibration methods are used for signals from real systems and from models, as Sekhar in [7] and Mancilla in [8]. Other studies have collected data during the run up or run down of a rotor. It has been shown that a cracked rotor produces a wide frequency band near the critical speed with violent oscillations, and that this phenomenon can be used for crack detection [9]. According to Mancilla's results, using a modified Jeffcott rotor, the main effects of a crack are found in local resonances during the run up or run down of the rotor. These local resonances appear at around 1/2, 1/3, and 1/4 of the critical speed of a healthy axle at various crack-imbalance orientations.

Vibration methods use a range of approaches for signal analysis. Fast Fourier transform (FFT) and Hilbert transform have traditionally been used to observe changes in the response or in eigenfrequencies when a crack appears [10,11]. However, over the last years, new techniques (classified by Sabnavis et al. in [6] as "non-traditional methods") have been reported, including the use of fractal dimension [12] and the Wavelet transform (WT) [13]. The WT is a time-frequency tool that is especially effective in treating non-stationary signals and has become one of the most widely used techniques. Applications of the WT are increasing, and they are now used for speech recognition [14,15]; denoising [16]; electrocardiographs [17]; and diagnosis of cracked rotating elements [18] as bearings [19], gears [20], and beams [21,22].

The Wavelet Packet transform (WPT) [23] is one of the latest improvements of the WT. WPT coefficients are sometimes used directly as features because they yield reliable information about faults [24]. Energy calculated using this

tool has also been used as a crack indicator, as in [25,26].

However, to interpret the information produced and to detect faults in rotating machinery, a classification system is needed. Recently, intelligent classification systems such as neural networks [27], fuzzy logic [28], genetic algorithms [29] and support vector machines [30] have attracted considerable attention. The results of the classification system used can estimate the reliability of the technique. The reliability of the inspection method can be defined as the probability of detecting a crack within a certain range of sizes under specific conditions and procedures. This is usually represented via probability of detection (POD) curves [31], that are universally accepted to evaluate a diagnosis method. There are many ways to obtain POD curves in each case. Traditionally, non destructive testing (NDT) techniques have used two methods to obtain these probabilities: signal response and hit-miss [32]. Both methods use probabilistic techniques to obtain the POD curves. The signal-response method is used when the output of the inspection technique is a signal, and depending on its value the presence of a crack can be recognized. The hit-miss method is used in cases where the output information has only two possible values: if there is a defect or not (as visual inspection).

The technique proposed in this study uses the energy data obtained using the WPT. First, an analytical Jeffcott rotor model was constructed to reproduce approximately the shaft behavior under the experimental machine conditions. Frequency bands that show higher changes in energy when a crack appears were identified. Vibration signals were then obtained from the rotating machine at different levels of crack sizes in the shaft from incipient to severe, to attempt to match the theoretical and experimental results. Finally, the POD curves were generated using the signal response method.

2 Analytical Model: Jeffcott Rotor

Considerable effort has been put into understanding the dynamic behavior of cracked rotating machinery [33–35].

In the present study, the model selected to verify the monitoring and diagnostic system was based on the equation of motion of a Jeffcott rotor model [36]. This model has been widely used to investigate rub interactions, spontaneous side-banding and stability. Applications of the Jeffcott rotor model have been reported in a previous study [37], where the rotor was complemented with a snubber ring. The model used in this study and its coordinate system are shown in Figure 1.

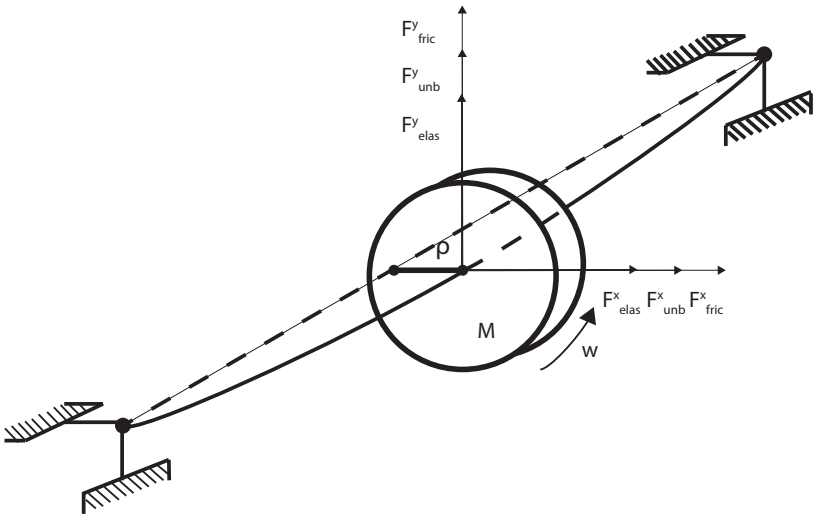

Fig. 1. Jeffcott rotor model and coordinate system.

The equations of the model [9] are given as

$$M\ddot{x} = F^x_{elas} + F^x_{unb} + F^x_{fric} \tag{1}$$

$$M\ddot{y} = F^y_{elas} + F^y_{unb} + F^y_{fric} \tag{2}$$

where F_{elas} represents elastic forces, F_{unb} unbalanced forces, and F_{fric} represents friction forces. The equations are shown in more detail as follows:

$$M\ddot{x} + c\dot{x} + kx - \frac{1}{2}g(\phi)[(\Delta k_1 + \Delta k_2\cos(2\phi)x + \Delta k_2\sin(2\phi))y] = M\rho\omega^2\cos(\varphi_0 + \omega t) \tag{3}$$

$$M\ddot{y} + c\dot{y} + ky - \frac{1}{2}g(\phi)[\Delta k_2\sin(2\phi))x + (\Delta k_1 - \Delta k_2\cos(2\phi)y] = M\rho\omega^2\sin(\varphi_0 + \omega t) \tag{4}$$

where M is the total mass of the shaft, c is the damping coefficient of the rotor, k the stiffness of the system, and ρ is the radius by which the center of the shaft is displaced from its axis. Moreover, g represents the change in the stiffness that a crack introduces into the shaft. This change is variable over time because of the breathing phenomena. Several models have been proposed to simulate this behavior, most of which only consider the maximum and minimum stiffness that occur when a crack is totally open and totally closed [38], represented by Δk_1 and Δk_2, respectively. Research is constantly providing new breathing functions [39]; however, the classical ones are the Gash function [40] and the Mayes and Davies function [41]. In this study, a modified Mayes and Davies function was used to simulate variations in the stiffness caused by the crack. New parameters are introduced to prevent the total closing of a crack, as shown in Eq.5.

$$g(\phi) = 0.8 * \frac{1 + \cos(\phi)}{2} + 0.2 \tag{5}$$

First, a healthy shaft was simulated, and acceleration measurements were performed. Three levels of cracks, corresponding to 12.5%, 25% and 50% of the shaft diameter ($D = 16mm$), were then added at mid-span. These depths were selected to cover a representative range of sizes, useful to extract conclusions about the more sensitive frequencies to the presence of a crack. The four conditions of cracks were modeled using a relative change of stiffness value for each crack size, corresponding to $\Delta k_1 = 0.0$ and $\Delta k_2 = 0.0$ for healthy shaft, $\Delta k_1 = 0.045 \cdot k$ and $\Delta k_2 = 0.011 \cdot k$ for a crack of 12.5%, $\Delta k_1 = 0.057 \cdot k$ and $\Delta k_2 = 0.024 \cdot k$ for a crack of 25%, and $\Delta k_1 = 0.095 \cdot k$ and $\Delta k_2 = 0.023 \cdot k$ for a crack of 50%.

The model was developed in $Matlab^{®}$ using properties of the shaft for which the experimental measurements were performed: $M = 0.378kg$, $c = 4.58N \cdot s/m$ (which represents a damping coefficient of $\xi = 0.003$), $k = 1544.3KN/m$, and $\rho = 2 \cdot 10{-}5m$.

Simulations were performed at steady state at rotational speeds: 20 Hz, 40 Hz and 60 Hz. The theoretical critical speed of the shaft was 321.7 Hz (the value obtained experimentally was 316.4 Hz). Thus the rotor could be considered rigid.

The number of points obtained for each signal was 2^{14}, with a sample frequency of 6 KHz.

3 Experimental Setup

Experimental measurements were performed for a rig comprising an aluminum shaft (based on the adimensional study characteristics of a railway axle scaled to 1/8), two ball bearings (ER10 from Rexnord) and a motor that drives the shaft through an elastic coupling. The shafts were tested in a healthy state, and then nine different levels of cracks (a) were induced by saw cuts. The values of a in Table 1 are expressed as the ratio between the crack depth d and shaft diameter D, where $D = 16mm$.

Defect level	1	2	3	4	5	6	7	8	9
Value ($a = d/D$)	0.04	0.08	0.12	0.17	0.22	0.28	0.33	0.42	0.5

Table 1
Crack depths a used for the experimental setup, expressed in relative terms with respect to the diameter of the shaft D.

The rig and an induced defect (level 2) are shown in Figure 2.

The rotational speed is controlled by an optical tachometer and was set to 20 Hz, 40 Hz and 60 Hz. The number of points for each measurement was 2^{14},

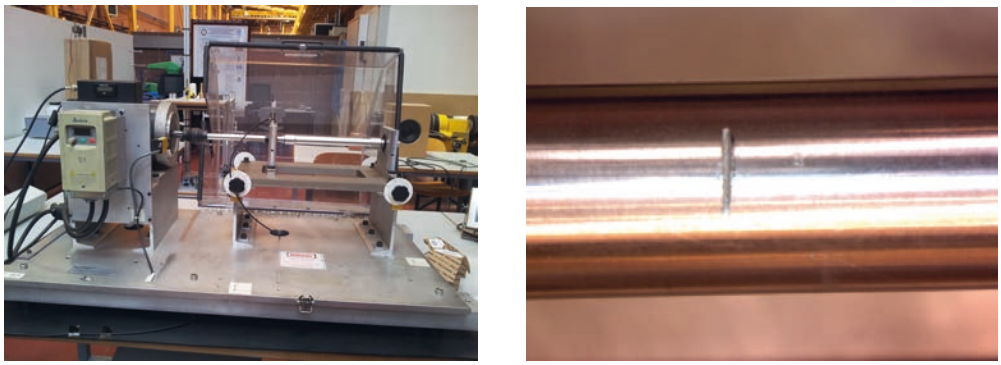

(a) (b)

Fig. 2. Fault simulation rig (a) and detail of an induced defect (b).

again with a sampling frequency of 6 KHz as in the analytical model.

For each fault condition and speed setting, 1,500 measurements are taken by groups of 100. To eliminate random noise, signals were averaged across 100 the samples obtained consecutively. Then, the number of measures to handle is 15 by condition.

4 Feature Extraction using WPT

The WT is especially efficient at performing local analysis of non-stationary signals. In the same manner that the FFT obtains correlation coefficients of a signal with a sinusoidal function, the WT obtains correlation coefficients of the signal and a mother wavelet. The WT extracts information in time and in frequency domains, and thus, it can locate in time the desired frequency components and detect discontinuities and transitory effects that the FFT misses. The discrete wavelet transform (DWT) is more commonly used than the continuous form of the WT because signals usually comprise discrete data and the computational cost is lower. Following Mallat [13], the DWT can be implemented via filters. Decomposition is performed by passing the signal through a low-pass filter g to obtain the wavelet approximation (A), and a high pass filter h to obtain the wavelet detail (D), as in Eq. 6 and Eq. 7.

$$A[n] = \sum_{k=-\infty}^{\infty} x[k]g[2n-k] \tag{6}$$

$$D[n] = \sum_{k=-\infty}^{\infty} x[k]h[2n-k] \tag{7}$$

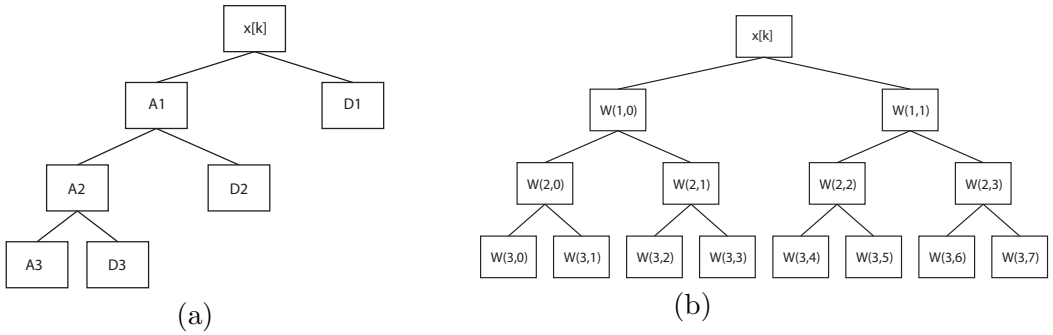

Fig. 3. Decomposition procedure for a signal x[k] to decomposition level 3 using (a) MRA analysis and (b) WPT analysis.

Several types of analysis are performed by the recursive application of the DWT. Decomposition halves the frequency band of the input; thus, following the Nyquist rule, it is necessary to downsample by two. The wavelet packets transform (WPT) was used to prevent problems associated with other tools based on the DWT, such as the multiresolution analysis (MRA), where the downsampling process can only be performed for the A information and not for the D information [42]. This results in a relatively lower spectral resolution at high frequencies and low temporal resolution at low frequencies. In contrast, the WPT allows A and D information to be decomposed recursively until the desired resolution. Examples of the results of decomposition using the MRA and WPT are shown in Figure 3.

Using WPT decomposition, $W(k, j)$ represents coefficients of the signal in each packet, k represents the decomposition level, and j represents the position of the packet within the decomposition level. Each correlation vector $W(k, j)$ has the structure given in Eq.8:

$$W(k, j) = \{w_1(k, j), ..., w_N(k, j)\} = \{w_i(k, j)\} \tag{8}$$

The concept of energy used in the WPT is similar to that used in the the FFT [24]. The energy of the packets can be obtained from the sum of the squares of the coefficients of each packet, given by Eq. 9:

$$E_{k,j} = \sum_i \{w_i(k, j)\}^2 \tag{9}$$

In this study, the "Daubechies 6" mother wavelet was used because of its proven effectiveness in this area [9]. The selected decomposition level determines the frequency resolution offered by each packet (same for all packets). Using a decomposition level of k, the number of packets obtained is 2^k. By considering the global frequency F (half of the sampling frequency according to the Nyquist theorem), the frequency resolution f_r of each packet is given

by Eq.10 [43]:

$$f_r = \frac{F}{2^k} \tag{10}$$

The value of f_r must be sufficiently small to prevent influence of other frequencies on the results. After preliminary studies of the computational cost, a value for f_r of 6 Hz was selected. The value of F is 3 KHz; thus, the nearest decomposition level is 9. Figure 4 shows an example of a temporal signal obtained from the rig (with a healthy shaft at 60 Hz) and its WPT decomposition at level 9.

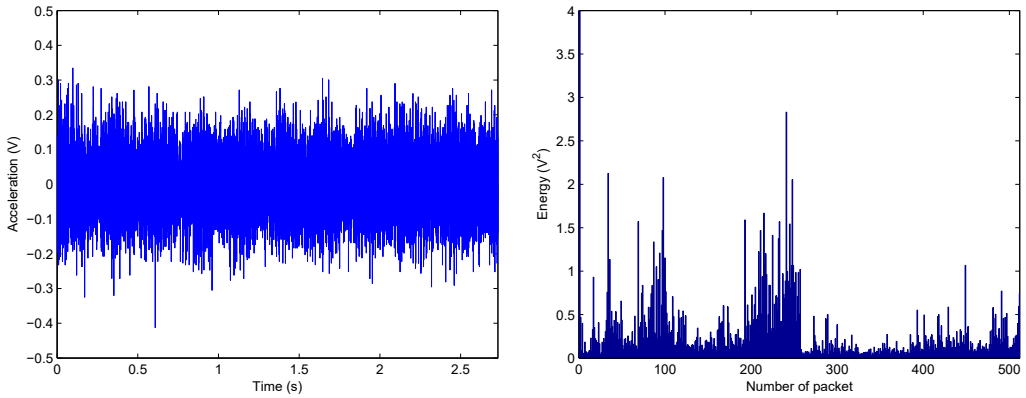

(a) (b)

Fig. 4. Example of a WPT signal obtained for a healthy axle at 60 Hz showing (a) temporal signal and (b) WPT decomposition at level 9 (512 energy packets)

5 Results and Discussion

WPT energies were calculated for all conditions measured for the signals obtained from the analytical model and experimental setup. The asolute values of the WPT energy differences between signals emitted from healthy and faulty axles were analyzed for each of the three speeds tested, as shown in Figure 5. Attention was paid to the first ten maximum differences obtained.

Signals obtained from the Jeffcott model can only be compared to the experimental ones qualitatively because the analytical model measured the acceleration at the center of the shaft at the middle section, whereas the experimental case signals were from vibration in the bearing housing. Thus, the amplitude and energyof the signals are not directly comparable.

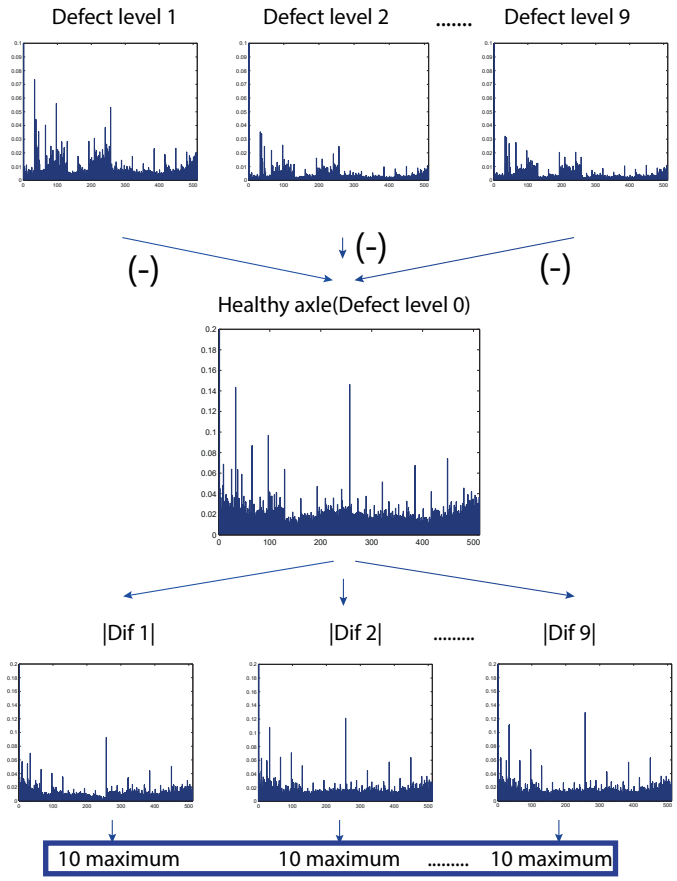

Fig. 5. Difference analysis procedure to detect increase in energy when a crack appears

5.1 WPT Energy Analysis

5.1.1 Analytical model results

First, a WPT energy analysis was performed for the signals obtained from the analytical model under all test conditions. Packets exhibiting larger differences when a crack appears were obtained. Increments of energy were significant at frequencies related to the first harmonics of the rotational speed (1x, 2x and 3x). This was observed for all three speeds tested.

At each speed, energy appeared to increase progressively with the severity of defect. Figure 6 shows the absolute energy increments for cracked condition signals regarding the healthy condition for the three first harmonics of the rotational speeds.

As can be concluded from Figure 6, the maximum absolute energy increments were found at 1x. The absolute energy increments were lower in 2x and further

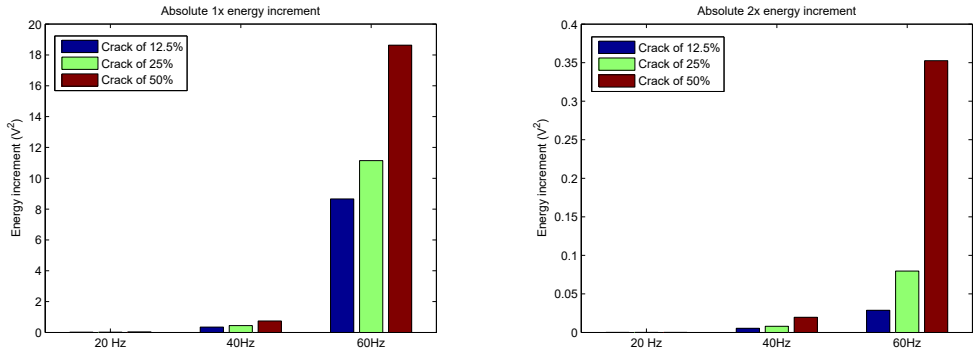

(a)

(b)

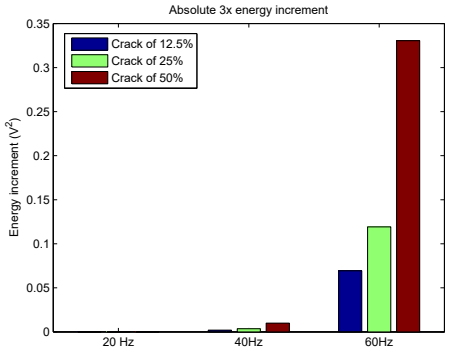

(c)

Fig. 6. Increments of energy regarding the healthy condition for the analytical model at the different rotational speeds (Hz) in packets related to (a) 1x frequency, (b) 2x frequency, and (c) 3x frequency.

lower at 3x, as derived from Eq. 11.

$$\Delta E_{abs}(1x) > \Delta E_{abs}(2x) > \Delta E_{abs}(3x) \tag{11}$$

The absolute energy increments depended strongly on the rotational speeds. When representing relative energy increments regarding the healthy condition, the dependence on the rotation speed is reduced, as can be observed in Figure 7.

In the case of relative energy increments, the highest increments were found at 3x. Lower values were observed at 2x and further lower at 1x, as derived from Eq. 12. This phenomenon can be attributed to the low 3x energy value for the healthy case.

$$\Delta E_{rel}(3x) > \Delta E_{rel}(2x) > \Delta E_{rel}(1x) \tag{12}$$

These results suggest that in relative terms, the energy increments when a crack appears are most significant at frequencies related to 3x. This contrasts

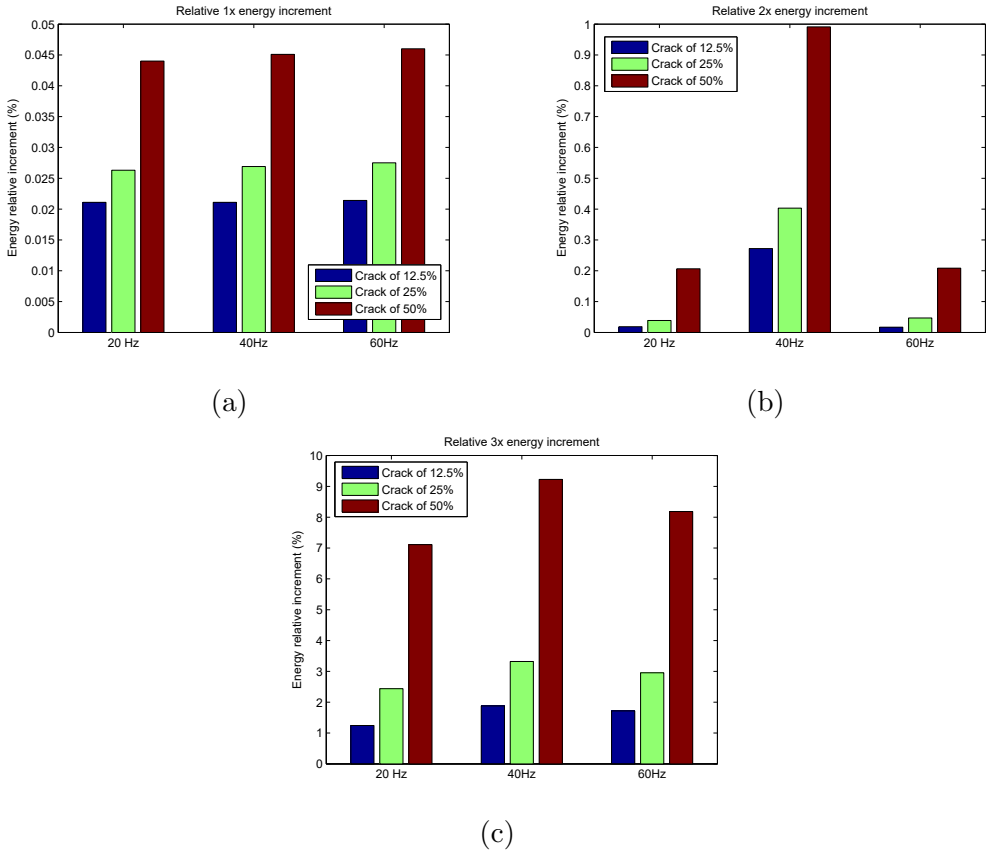

Fig. 7. Relative increments of energy regarding the healthy condition for the analytical model at different rotational speeds (Hz) found in packets related to (a) 1x frequency, (b) 2x frequency, and (c) 3x frequency.

with the case of the absolute increments and previous research, where it has been argued that the largest differences appear at 1x and 2x frequencies.

5.1.2 Experimental results

The same procedure was next applied to the experimental study. First the absolute energy increments were calculated with respect to the healthy axle. The number of measurements to handle was 15 by each case, and all combinations were analyzed. The frequency bands that showed repeatable energy increments are given in Table 2.

As can be observed in Table 2, the frequency bands that serve as as accurate indicators of a crack are related to 3x. The effects of a crack are hidden at 1x and 2x and no increase in energy was found with repeatability. This is consistent with previous research [6]. This can be attributed to the existence of other defects, such as misalignment or bending, which obscured the effects of the crack.

Rotation speed (Hz)	Significative frequency bands (Hz)
20	58.6-64.5 (3x)
40	117.2-123 (3x)
60	175.8-181.6 (3x)

Table 2
Representative frequency bands regarding changes in energy with respect to healthy axle for experimental case

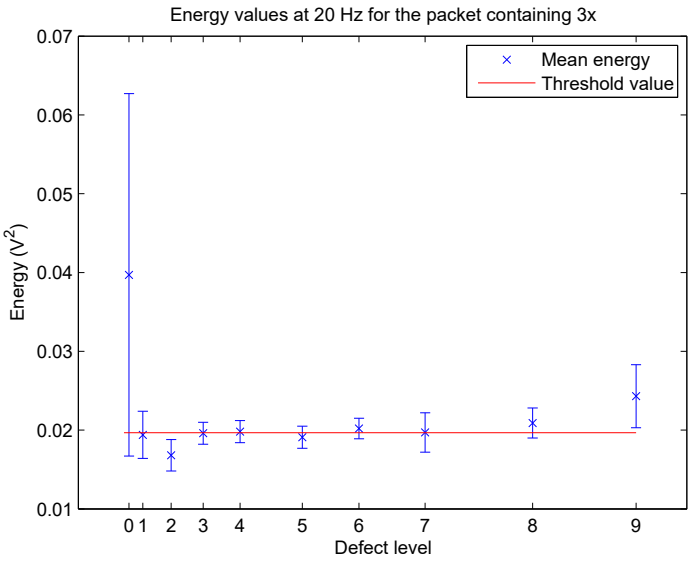

Fig. 8. Energy distributions in frequency bands related to 3x (represented by mean and standard deviation) versus the level of crack at 20 Hz.

The energy distributions in the significant frequency bands at all speeds were analyzed in terms of mean values and standard deviations. Figures 8, 9 and 10 show energy distribution vs. crack size at all tested speeds, with a proposed threhold value to separate data for healthy and from cracked shafts.

The most important changes in energy were observed at 60 Hz. At 20 Hz, no significant increase in energy was detected, and the standard deviation for the healthy axle was very high to permit reliable crack detection. At 40 and 60 Hz, the energy of the packet containing 3x is strongly influenced by the crack size. In both cases, when the crack size increases, energy increases. However, the effects are greater at 60 Hz.

These results show that the speed is critical for the inspection. When the speed increases, the effects of the crack become more visible, with the clearest results being recorded at 60 Hz. This can be attributed to noise effects. When the speed increases, the amplitude of vibrations is larger; thus, the signal to noise ratio is also higher.

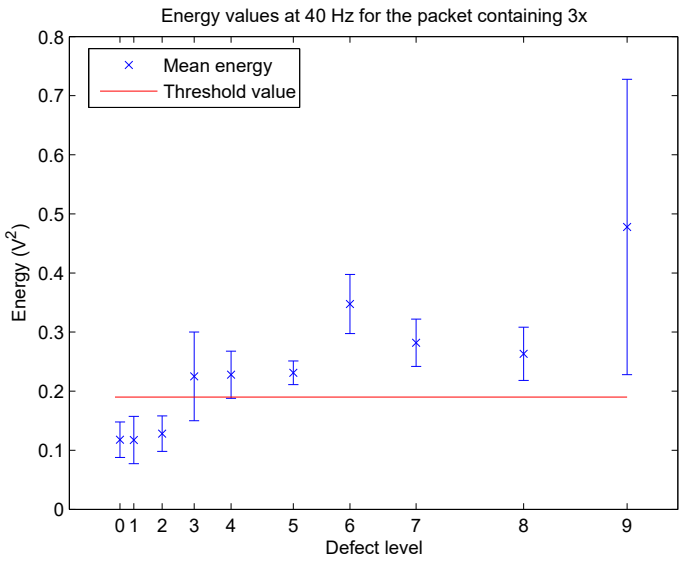

Fig. 9. Energy distributions in frequency bands related to 3x (represented by mean and standard deviation) versus the level of crack at 40 Hz

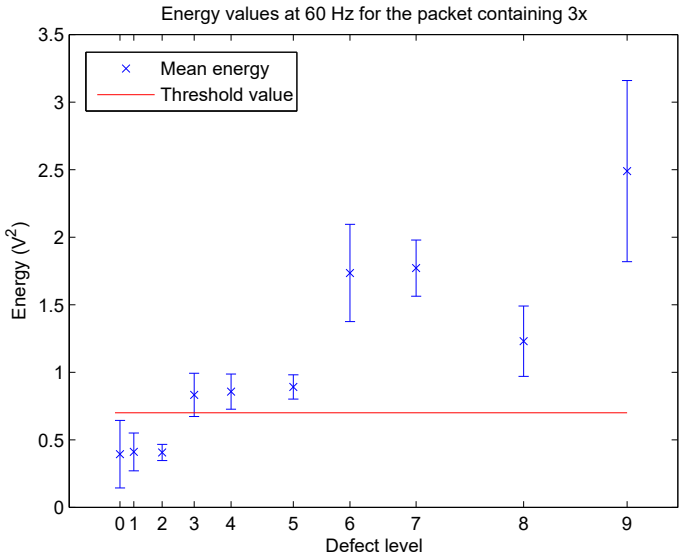

Fig. 10. Energy distributions in frequency bands related to 3x (represented by mean and standard deviation) versus the level of crack at 60 Hz

At rotational speeds of 40 Hz and 60 Hz (where the energy levels are most strongly affected by the crack size), three zones can be distinguished. The first zone comprises the healthy axle and defect levels 1 and 2; their mean values are very similar, standard deviations are low, and crack sizes do not trigger rises in energy compared to the healthy condition. The second zone comprises defect levels 3, 4 and 5, where a step change in the energy can be observed compared to the first zone. Defect levels 3, 4 and 5 have very similar mean values and standard deviations are low. They cannot be distinguished from

	k	β	*R-square*
Theoretical 3x fitting	0.063	3.57	0.99
Experimental 3x fitting	0.39	3.51	0.91

Table 3
Values of fitting to exponential functions of theoretical and experimental energies related to 3x at 60 Hz.

each other but can be clearly differentiated from the first zone. The third zone comprises defect levels 6, 7, 8, and 9, where a disorderly behavior is observed in the means of the energy values, and the standard deviations are higher. This zone is clearly differentiated from the first and second in terms of energy values.

It was next attempted to establish whether the recorded values can be approximated to a unique known curve to gain a qualitative understanding of the evolution of the system and to compare the experimental results with the theoretical ones.

5.2 Fitting energy levels at 3x vs crack size

A curve-fitting analysis was performed for the energies at 3x plotted against the defect level. The analysis was performed for the rotational speed of 60 Hz, for which the results where the sharpest.

The first fitting used the signals obtained from the analytical model for the packet containing the 3x component. An *R-square* (or correlation value) of 0.99 was obtained using an exponential function of the type in Eq. 13.

$$\hat{a} = k \cdot \exp(\beta \cdot a) \tag{13}$$

By performing the same analysis for the experimental signals acquired at 60 Hz, it was found that the best fits were again obtained using exponential functions. The fittings for theoretical and experimental signals are shown in Figure 11.

Table 3 shows the values of k, β, and *R-square* value for all fittings performed.

As can be observed, there were large differences between the experimental and theoretical data. This was expected because theoretical signals measure vibrations at the center of the shaft, whereas experimental signals are obtained from the bearing housing. The amplitudes can therefore be very different. However, the value of β is very similar (at around 3.5) for the theoretical and experimental data. The conclusion of this analysis is that the *R-square* values

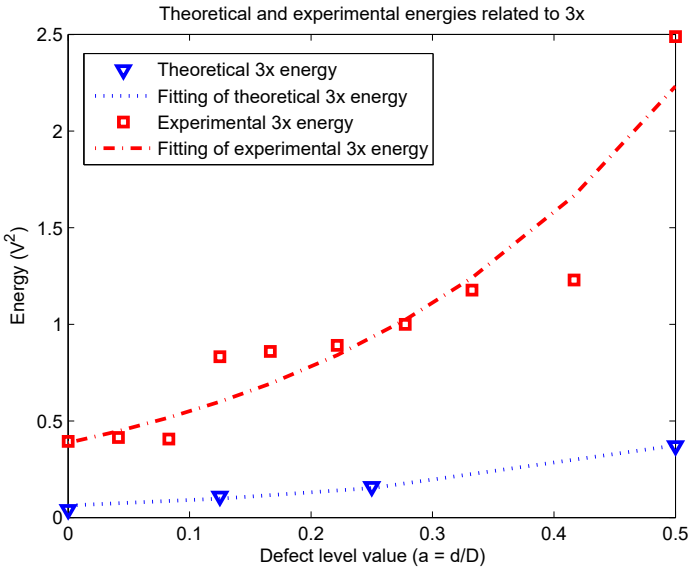

Fig. 11. Theoretical and experimental energies related to 3x at 60 Hz fitted to exponential functions.

are large in all cases, confirming that the energies at 3x can be approximated to an exponential function, where k and β values depend on the nature of the mechanical system.

5.3 POD calculation

To translate the energy data at different crack sizes into POD curves, the signal-response method was used. The method, imported from NDT, assumes that the energy level (result of the inspection) increases exponentially with the crack size, i.e., there is a correlation between the logarithm of the response $\hat{a}$ and that of the crack size a [44]:

$$\ln(\hat{a}) = \alpha + \beta \cdot \ln(a) + \gamma \tag{14}$$

where γ represents an error distribution with a mean of zero and a constant standard deviation σ_γ. Equation 14 assumes that $ln\hat{a}$ has a normal distribution according to $N(\mu(a), \sigma_\gamma^2)$, i.e., with mean $\mu(a) = \alpha + \beta \cdot \ln(a)$ and standard deviation σ_γ. Therefore, the inspection data have a log-normal distribution [45,32]. A threshold value $\hat{a}_{th}$ is established, and when it is exceeded, a crack is assumed to be initiated. Accordingly, the probability of detection of a crack of size a, can be expressed by Eq. 15:

$$POD(a) = Pr[\ln(\hat{a} > \ln(\hat{a}_{th}))] \tag{15}$$

This also can be expressed as Eq. 16:

$$POD(a) = 1 - F\left\{\frac{\ln(\hat{a}_{th}) - [\alpha + \beta \cdot \ln(a)]}{\sigma_\gamma}\right\} \tag{16}$$

where F is the cumulative function of the normal distribution.

On the basis of the above data analysis, it can be assumed that our responses follow a log-normal distribution, thereby allowing POD curves to be generated. The POD curve at 60 Hz for the packet containing the 3x component at a confidence limit of 95% is shown in figure 12. This was derived using a threshold value of 0.7.

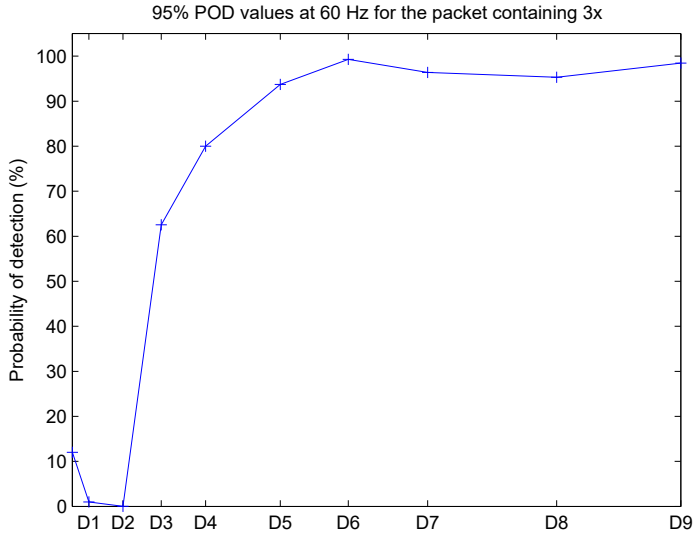

Fig. 12. POD curve at 60 Hz for the packet containing the 3x component at the 95% confidence lower limit.

6 Conclusions

This study presents a novel technique for the detection of cracks in rotating machinery based on a WPT energy analysis. Vibration signals were obtained from an analytical Jeffcott rotor model, and a WPT energy analysis was performed. It was shown that 1x, 2x and 3x energy levels rise significantly as a crack initiates and grows. Experimental measurements were also performed for under a range of fault conditions and at different steady-state rotational speeds. The results of the WPT energy analysis matched the theoretical and experimental results at the 3x rotational speed. The theoretical and experimental results show that the energy level at this frequency increases exponentially when plotted against crack size. POD curves at the 95% lower confidence

limit confirmed that the reliability of the method improves as the rotational speed increases. At 60 Hz, cracks with depths greater than 12% of the shaft diameter can be detectedwith high reliability.

The technique has applications in condition monitoring under stationary conditions. It allows to establish parameters of a machine under normal operating conditions and to detect the presence of a crack if a threshold value is exceeded.

7 Acknowledgements

The authors would like to thank the Spanish Government for financing through the CDTI project RANKINE21 IDI-20101560.

References

[1] C. Papadopoulos, The strain energy release approach for modeling cracks in rotors: A state of the art review, Mechanical Systems and Signal Processing 22 (2008) 763–789.

[2] N. Bachschmid, P. Penacci, Editorial. crack effects in rotordynamics, Mechanical Systems and Signal Processing 22 (2008) 761–762.

[3] A. Sekhar, Identification of unbalance and crack acting simultaneously in a rotor system: Modal expansion versus reduced basis dynamic expansion, Journal of Vibration and Control 11 (9) (2005) 1125–1145.

[4] P. Pennacchi, N. Bachschmid, A. Vania, A model-based identification method of transverse cracks in rotating shafts suitable for industrial machines, Mechanical Systems and Signal Processing 20 (8) (2006) 2112–2147.

[5] Z. Kulesza, J. Sawicki, Rigid finite element model of a cracked rotor, Journal of Sound and Vibration 331 (2012) 4145–4169.

[6] G. Sabnavis, R. Kirk, M. Kasarda, D. Quinn, Cracked shaft detection and diagnostics: a literature review, The Shock and Vibration Digest 36) (2004) 287–296.

[7] A. Sekhar, B. Prabhu, Crack detection and vibration characteristics of cracked shafts, Journal of Sound and Vibration 157 (2) (1992) 375–381.

[8] J. Gomez-Mancilla, J. Sinou, V. Nosov, The influence of crack-imbalance orientation and orbital evolution for an extended cracked jeffcott rotor, Comptes Rendus Mecanique 332 (12) (2004) 995–962.

[9] C. Castejón, J. García-Prada, M. Gómez, J. Meneses, Automatic detection of cracked rotors combining multiresolution analysis and artificial neural networks, Journal of Vibration and Control, D.O.I. 10.1177/1077546313518816.

[10] A. Sekhar, On-line rotor fault identification by combined model and signal based approach, Noise and Vibration Worldwide 35 (7) (2004) 16–30.

[11] M. Feldman, S. Seibold, Damage diagnosis of rotors: application of hubert transform and multihypothesis testing, Journal of Vibration and Control 5 (3) (1999) 421–442.

[12] L. Hadjileontiadis, E. Douka, A. Trochidis, Fractal dimension analysis for crack identification in beam structures, Mechanical Systems and Signal Processing 19(3) (2005) 659–674.

[13] S. Mallat, A wavelet tour of signal processing, Academic Press, 1998.

[14] L. Vignolo, D. Milone, H. Rufiner, Genetic wavelet packets for speech recognition, Expert Systems with Applications.

[15] E. Avci, Z.H.Akpolat, Speech recognition using a wavelet packet adaptive network based fuzzy inference system, Expert Systems with Applications 31 (3) (2006) 495–503.

[16] P. Mercorelli, A denoising procedure using wavelet packets for instantaneous detection of pantograph oscillations, Mechanical Systems and Signal Processing 35 (1-2) (2013) 137–149.

[17] M. Tinati, B. Mozaffary, A wavelet packets approach to electrocardiograph baseline drift cancellation, International Journal of Biomedical Imaging (2006) 1–9.

[18] Z. Peng, Application of the wavelet transform in machine condition monitoring and fault diagnostics: a review with bibliography, Mechanical Systems and Signal Processing 18 (2004) 199–221.

[19] X. Lou, K. Loparo, Bearing fault diagnosis based on wavelet transform and fuzzy inference, Mechanical Systems and Signal Processing (2004) 1077–1095.

[20] W. Wang, P. McFaden, Application of wavelets to gearbox vibration signals for fault detection, Journal of Sound and Vibrationl 192 (1996) 927–939.

[21] A. Gentile, A. Messina, On the continuous wavelet transforms applied to discrete vibrational data for detecting open cracks in damaged beams, Journal of Solid and Structures 40 (2003) 295–315.

[22] E. Douka, S. Loutridis, A. Trochidis, Crack identification in beams using wavelet analysis, International Journal of Solids and Structures 40 (2003) 3557–3569.

[23] B. Liu, S. Ling, Machinery diagnostic based on wavelet packets, Journal of vibration and control 3 (1997) 5–17.

[24] Q. Hu, Z. He, Z. Zhang, Y. Zi, Fault diagnosis of rotating machinery based on improved wavelet package transform and svms ensemble, Mechanical system and signal processing 21 (2007) 688–705.

[25] Y. Feng, F. Schlindwein, Normalized wavelet packets quantifiers for condition monitoring, Mechanical Systems and Signal Processing 23 (2009) 712–723.

[26] C. Castejón, M. Gómez, J. García-Prada, A. Ordonez, H. Rubio, Automatic selection of the WPT decomposition level for condition monitoring of rotor elements based on the sensitivity analysis of the wavelet energy, International Journal of Acoustics and Vibration.

[27] R. Walker, R. Vayanat, S. Perinpanayagam, I. Jennions, Unbalance localization trough machine nonlinearities using an artificial neural network approach, Mechanism and Machine Theory 75 (2014) 54–66.

[28] M. Laribi, A. Mlika, L. Romdhane, S. Zeghloul, A combined genetic algorithm-fuzzy logic method (ga-fl) in mechanism synthesis, Mechanism and Machine theory (39) (2004) 717–735.

[29] S. Singh, R. Tiwari, Identification of a multi-crack in a shaft system using transverse frequency response functions, Mechanism and Machine Theory 45(12) (2010) 1813–1827.

[30] A. Widodo, B. Yang, Support vector machine in machine condition monitoring and fault diagnosis, Mechanical Systems and Signal Processing 21(6) (2007) 2560–2574.

[31] W. Rummel, Recommended practice for demonstration of non destructive evaluation (NDE) reliability in aircraft parts, Materials Evaluation 40 (1982) 923–932.

[32] S. Cantini, S. Beretta, Structural reliability assessment of railway axles, Lucchini RS, 2011.

[33] Y. Ishida, Cracked rotors: Industrial machine case histories and nonlinear effects shown by simple jeffcot rotor, Mechanical Systems and Signal Processing 22 (2012) 805–817.

[34] C. Stoisser, S. Audebert, A comprehensive theoretical, numerical and experimental approach for crack detection in power plant rotating machinery, Mechanical Systems and Signal Processing 22 (2012) 818–844.

[35] C. Kumar, V. Rastogi, A brief review on dynamics of a cracked rotor, International Journal of Rotating Machinery.

[36] L. Cveticanin, Free vibration of a jeffcott rotor with pure cubic non-linear elastic property of the shaft, Mechanism and Machine Theory 40 (2005) 1330–1344.

[37] E. Karpenko, M. Wiercigroch, E. Pavlovskaia, R. Neilson, Experimental verification of jeffcott rotor model with preloaded snubber ring, Journal of Sound and Vibration 298 (2006) 907–917.

[38] P. Saavedra, D. Baquedano, L. S. Juan, Modelo numerico para el estudio dinamico de un rotor con eje agrietado, Revista Internacional de Metodos Numericos para el Calculo y Diseno en Ingenieria 2 (1996) 125–146.

[39] M. Al-Shudeifat, E. Butcher, New breathing functions for the transverse breathing crack of the cracked rotor system: Approach for critical and subcritical harmonic analysis, Journal of Sound and Vibration 330 (2011) 526–544.

[40] R. Gash, Dynamic behavior of a simple rotor with a cross-sectional crack (1976).

[41] I. Mayes, W. Davies, Analysis of the response of a multi-rotor bearing system containing a transverse crack in a rotor, Journal of Vibration Acoustics Stress and Reliability in Design Transactions of ASME.

[42] A. Jensen, A. la Cour-Harbo, Ripples in Mathematics, Springer, 2000.

[43] M. Gómez, C. Castejón, J. García-Prada, Incipient Fault Detection in Bearings through the use of WPT energy and Neural Networks, Advances in Condition Monitoring of Machinery in Non-Stationary Operations. Lecture Notes in Mechanical Engineering, 2014.

[44] G. Georgiou, Probability of detection (pod) curves: derivation, applications and limitations, in: HSE Books, Health and Safety, Executive, UK, no. Research Report 454, 2006.

[45] P. N. Bachschmid, P, E. Tanzi, Cracked rotors: A survey on Static and Dynamic Behaviour Including Modelling and Diagnosis, Springer, 2010.